

Article

Effect of CeO₂ Content on Microstructure and Properties of Ni-Based Tungsten Carbide Layer by Plasma Arc Cladding

Juan Pu^{1,2,*} , Yu-Bo Sun¹, Lei Wu¹, Peng He² and Wei-Min Long³

¹ School of Materials Science and Engineering, Jiangsu University of Science and Technology, Zhenjiang 212003, China; suyub_513@163.com (Y.-B.S.); wulei1652258026@163.com (L.W.)

² State Key Laboratory of Advanced Welding and Joining, Harbin Institute of Technology, Harbin 150001, China; hithepeng@hit.edu.cn

³ Zhengzhou Research Institute of Mechanical Engineering, Zhengzhou 450001, China; brazelong@163.com

* Correspondence: pu_juan84@163.com

Abstract: A Ce-containing Ni-based tungsten carbide layer was prepared on the surface of Q345 steel by plasma arc cladding technology. The effect of CeO₂ additions on the microstructure and properties of the Ni-based tungsten carbide cladding layer was investigated. The results showed that the Ni-based tungsten carbide cladding layer had no pores and cracks and that their microstructural composition remained unchanged with CeO₂ in the powder. After adding CeO₂ into the powder, Ce atoms were absorbed on the surface of tungsten carbide particles to promote their dissolution and spheroidization. The preferentially formed high-melting-point Ce₂O₃ acted as a nucleating agent to induce the formation and dispersion of carbides. The shape of carbide particles changed from an irregular shape to a spherical shape. When the content of CeO₂ was less than 0.2 wt.%, with the increase of CeO₂ additions, the microstructure was refined. Meanwhile, the hardness and wear resistance of Ni-based tungsten carbide cladding layer increased. When the content of CeO₂ was 0.2 wt.%, the refinement effect of CeO₂ on the microstructure reached an optimum value, and the hardness value reached the maximum of 1139 HV₁₀. Moreover the wear resistance was the best. This was attributed to the dispersion strengthening of undissolved tungsten carbide particles, the solid solution strengthening of Ni-based solid solution, and the precipitation strengthening of carbides. However, as the content of CeO₂ exceeded 0.2 wt.%, excessive CeO₂ increased the viscosity of the solution, resulting in component segregation. Thus, the refinement and spheroidization action of CeO₂ weakened, and irregular-shaped carbides appeared again. The hardness and wear resistance of the Ni-based tungsten carbide cladding layer obviously decreased. Ce-containing Ni-based tungsten carbide layer can be widely used in deep-sea mining and other fields due to its high hardness and wear resistance.

Keywords: plasma arc cladding; Ni-based tungsten carbide coating; CeO₂ addition; microstructure; property



Citation: Pu, J.; Sun, Y.-B.; Wu, L.; He, P.; Long, W.-M. Effect of CeO₂ Content on Microstructure and Properties of Ni-Based Tungsten Carbide Layer by Plasma Arc Cladding. *Coatings* **2022**, *12*, 342. <https://doi.org/10.3390/coatings12030342>

Academic Editor: Nazlim Bagcivan

Received: 9 February 2022

Accepted: 28 February 2022

Published: 6 March 2022

Publisher's Note: MDPI stays neutral with regard to jurisdictional claims in published maps and institutional affiliations.



Copyright: © 2022 by the authors. Licensee MDPI, Basel, Switzerland. This article is an open access article distributed under the terms and conditions of the Creative Commons Attribution (CC BY) license (<https://creativecommons.org/licenses/by/4.0/>).

1. Introduction

In order to implement the circular economy promotion law, the central government issued opinions on promoting the development of the remanufacturing industry in May 2010. Remanufacturing, as a new type of industry, uses surface engineering technology and other processing technologies to repair the shape, size, and performance of parts. It prolongs the service life of parts so as to reduce the environmental pollution and waste caused by parts' damage. This is of great significance to economic and social development [1–3]. Plasma arc cladding technology is a surface modification technology which uses plasma arc as the heat source to melt powder or wire on the surface of the substrate, achieving a metallurgical combination between the cladding layer and substrate. Plasma arc cladding technology received attention from the remanufacturing industry due to its

The mixed alloy powder was cladded on the surface of Q235 steel plate by using DML-V03AD microbeam plasma-arc equipment (Shanghai Duomu Industry, Shanghai, China). The process parameters were selected as follows: the ion gas flow rate was 1.0 L/min, the shielding gas flow rate was 15 L/min, the powder providing gas flow rate was 4 L/min, the powder feeding speed was 18 cm³/min, the cladding speed was 2 mm/s, the current was 80 A, and the height from nozzle to workpiece was 10 mm. The size of Ni-based tungsten carbide layer obtained by plasma arc cladding technology was 80 mm × 14 mm × 4 mm.

The samples were intercepted by wire cutting along the direction perpendicular to the cladding layer. After grinding and polishing, the metallographic specimen with the size of 10 mm × 10 mm × 10 mm was etched with a mixture of boiling nitric and hydrochloric acids for 15 s. The microstructure of the cladding layer was observed by a ZEISS optical microscope (OM, Jena, Germany) and a JSM-6480 scanning electron microscope (SEM, JEOL, Tokyo, Japan). The chemical composition of characteristic points in microstructure was tested by an energy dispersive spectrometer (EDS, Carl Zeiss, Jena, Germany). The phase composition of cladding layer with the size of 10 mm × 10 mm × 3 mm was analyzed by an XRD-6000 X-ray diffractometer instrument (XRD, Shimadzu, Kyoto, Japan) with Cu-K_α radiation and scanning angles (2θ) between 10° and 90°.

The hardness of the cladding layer was measured by a Vickers hardness tester (KB30s, KB, Munich, Germany). The test load was 100 N. A point was hit every 0.5 μm along the direction perpendicular to the fusion line, and the reported values were an average of five data points in the same horizontal direction.

The pin-disc dry sliding friction and wear test of the sample was carried out with universal friction and wear tester (MMW-1, Jinan Chenda, Jinan, China). GCr15 quenched bearing steel with a hardness of 62 HRC was selected as the grinding disc. The pin size of the cladding layer was φ5 × 15 mm while the size of the grinding disc was φ52 × 7 mm. All of the cladding samples were ground and polished before doing the wear test. The wear test parameters were the load of 100 N, the rotating speed of 100 r/min and the experimental time of 900 s. After the wear test, the wear loss weight of the cladding layer was measured by an electronic analysis balance (BSM-220.4, Shanghai Zhuojing, Shanghai, China) with the precision of 0.01 mg. The mass before wear was recorded as m_1 , the mass after wear was m_2 , the wear distance was L , and the wear rate was $A = (m_1 - m_2)/L$. The wear morphology of the cladding layer was observed by JSM-6480 scanning electron microscope (SEM, JEOL, Tokyo, Japan) to analyze its wear mechanism.

3. Results and Analysis

3.1. Effect of CeO₂ Content on Microstructure of Ni-Based Tungsten Carbide Cladding Layer

3.1.1. Microstructure Analysis of Ni-Based Tungsten Carbide Cladding Layer

Figure 1a–e shows the microstructure in the cross section of Ni-based tungsten carbide plasma cladding layer under different CeO₂ contents. Figure 1a₁–e₁ presents the corresponding local enlarged drawing. When the alloy powder was CeO₂-free, the microstructure of the cladding layer was mainly composed of dark grey Ni-based matrix and white tungsten carbide particles. Moreover, the tungsten carbide particles were mainly deposited at the bottom of the cladding layer (see Figure 1a,a₁). After adding CeO₂ into the alloy powder, the microstructure of the cladding layer was composed of Ni-based matrix, undissolved tungsten carbide particles and secondary precipitated carbides (see Figure 1b–e₁). If the content of CeO₂ was no more than 0.2 wt.%, the number of tungsten carbide particles decreased gradually while the number of secondary precipitation carbide increased gradually with the increase of CeO₂ content. The shape of the tungsten carbide particles changed from irregular type to spherical type. The secondary precipitation carbide was fine and distributed uniformly in the matrix. This suggested that CeO₂ played the role of refinement and spheroidization. When the CeO₂ content was 0.2 wt.% (see Figure 1c,c₁), all of the carbides were finest. However, when the CeO₂ content was increased to 0.5 wt.% (see Figure 1d,d₁) and 1.0 wt.% (see Figure 1e,e₁), the secondary precipitated carbide changed from spherical type to rods or bars while tungsten carbide particles showed ir-

regular. It indicated that excessive CeO_2 weakened its role in spheroidizing and refining carbides. Therefore, the optimal content of CeO_2 was 0.2 wt.%.

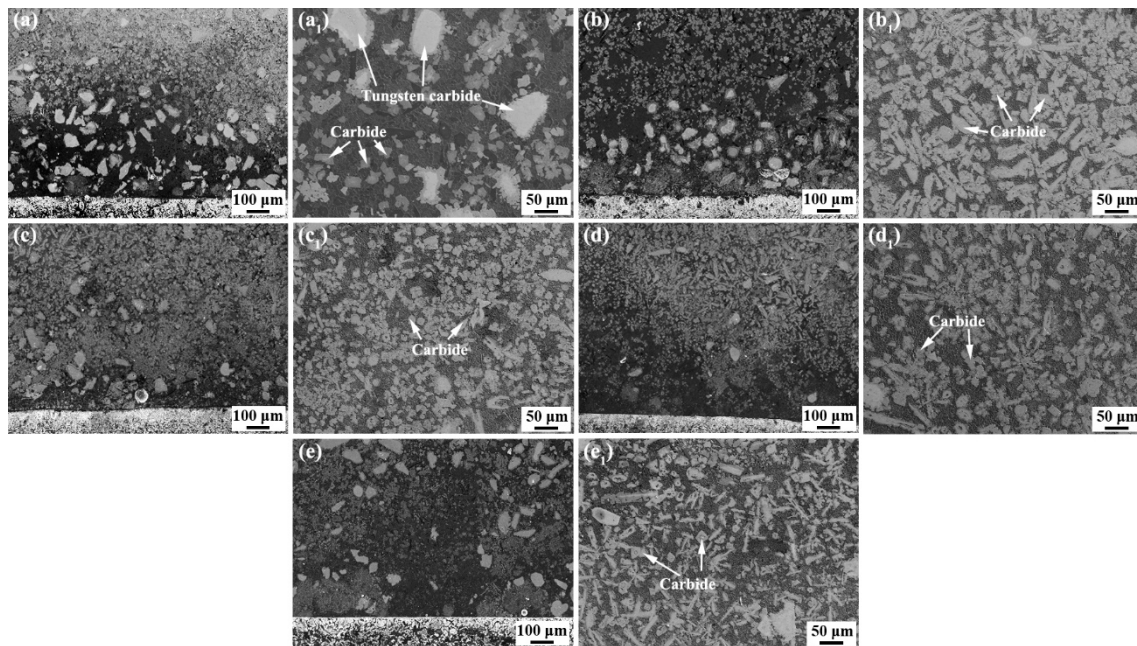


Figure 1. Microstructure in cross section of Ni-based tungsten carbide cladding layer under different CeO_2 contents: (a,a₁) 0 wt.% CeO_2 , (b,b₁) 0.1 wt.% CeO_2 , (c,c₁) 0.2 wt.% CeO_2 , (d,d₁) 0.5 wt.% CeO_2 , and (e,e₁) 1.0 wt.% CeO_2 .

Figure 2 shows the average area of carbides in the cladding layer measured by the quantitative metallography analysis system. When the powder did not contain CeO_2 , the average area of carbides in the cladding layer was $2732 \pm 35 \mu\text{m}^2$, and the standard deviation was 1034. With the increase of CeO_2 addition in the powder, the average area of carbides decreased first and then increased slightly. As the CeO_2 content was 0.2 wt.%, the average area and standard deviation of carbides reached the minimum, which was $892 \pm 35 \mu\text{m}^2$ and 301, respectively. When the CeO_2 content was 1.0 wt.%, the average area of carbides was $1237 \pm 35 \mu\text{m}^2$ and the standard deviation was 594. The results show that adding 0.2 wt.% CeO_2 into the powder can refine the carbide and improve its uniformity in the cladding layer, which confirmed the result in Figure 1.

In order to determine the phase composition of the cladding layer, the sample was analyzed by XRD diffraction (as shown in Figure 3). Whether CeO_2 was added to the powder or not, the cladding layer was mainly composed of γ -Ni solid solution, M_{23}C_6 ($\text{M} = \text{Cr}, \text{Fe}, \text{Ni}, \text{W}$). The addition of CeO_2 mainly affected the diffraction peak intensity of M_{23}C_6 carbides. After adding CeO_2 into the powder, the high melting point Ce-containing compounds can act as the heterogeneous nucleation core to promote the formation of carbides.

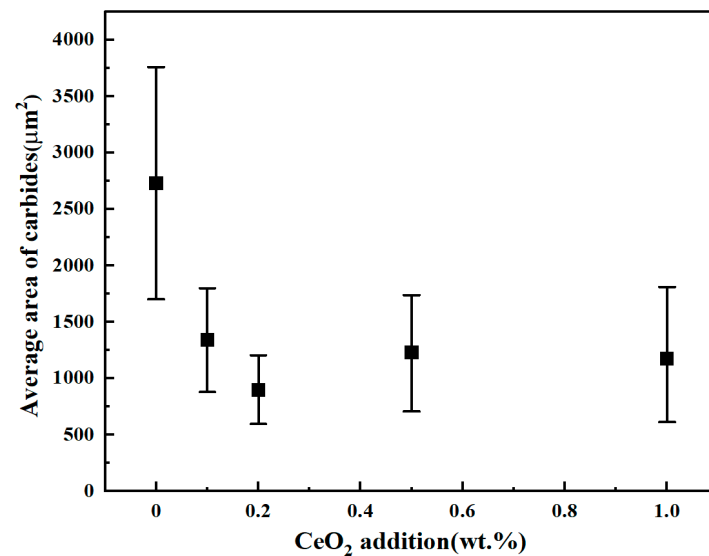


Figure 2. The average area of carbides in Ni-based tungsten carbide cladding layer under different CeO₂ addition.

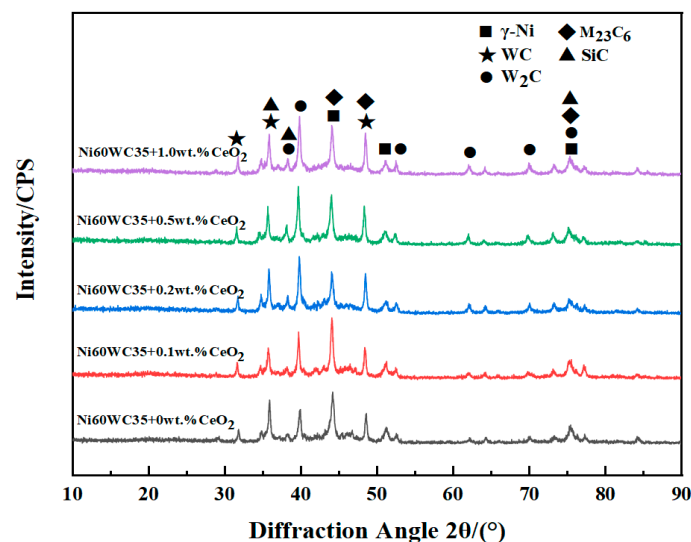


Figure 3. X-ray diffraction results of the Ni-based tungsten carbide cladding layer under different CeO₂ contents.

3.1.2. Action Mechanism of CeO₂ in Ni-Based Tungsten Carbide Cladding Layer

Figure 4 shows the morphology of the tungsten carbide and its surrounding structures in the cladding layer under different CeO₂ contents. When the powder did not contain CeO₂, the shape of the tungsten carbide was irregular, the edge of tungsten carbide produced microcracks, and the tungsten carbide particles were locally dissolved (as shown in Figure 4a). After adding 0.1 wt.% CeO₂ into the powder, the size of tungsten carbide decreased and its shape became spherical, while the tungsten carbide particles started to dissolve (see Figure 4b). When the CeO₂ content in the powder was 0.2 wt.%, the number of secondary precipitated carbides that surrounded tungsten carbide particles increased and they distributed uniformly in the cladding layer (see Figure 4c). As the CeO₂ content was raised to 0.5 wt.% and 1.0 wt.%, the carbides that surrounding tungsten carbide particles started to grow slightly (see Figure 4d,e), and the tungsten carbide gradually became irregular again (see Figure 4e). In order to clarify the action mechanism of CeO₂ on tungsten carbide and carbides in the cladding layer, EDS analysis was performed. The EDS results of spectrum 1, 2, 3 in Figure 4a and spectrum 4, 5, 6 in Figure 4e listed in Table 2.

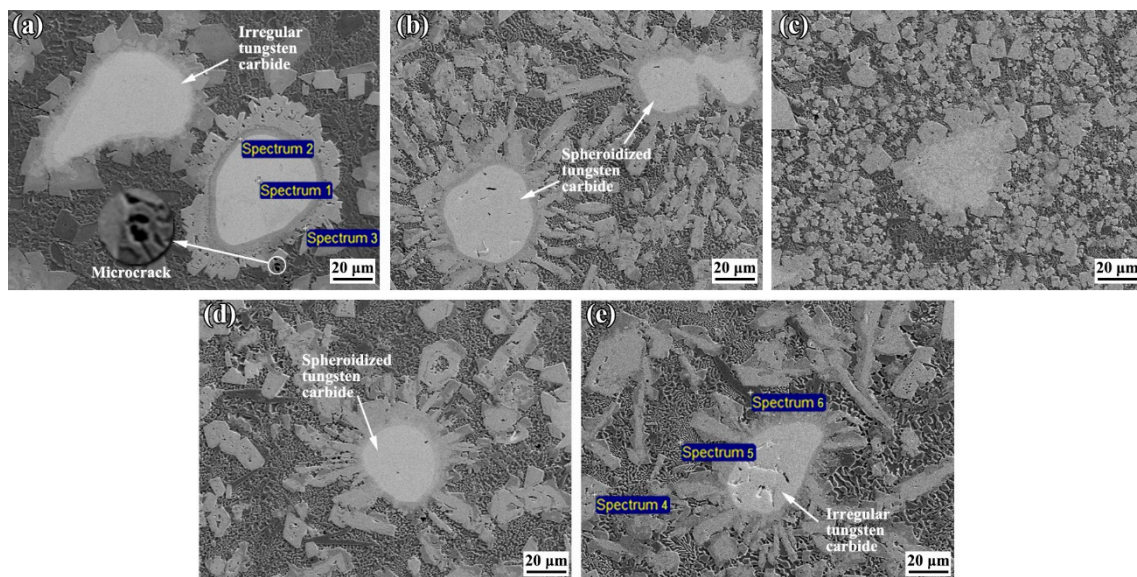


Figure 4. Morphologies of tungsten carbide particles and its surrounding in the cladding layer under different CeO_2 contents: (a) 0 wt.% CeO_2 , (b) 0.1 wt.% CeO_2 , (c) 0.2 wt.% CeO_2 , (d) 0.5 wt.% CeO_2 , and (e) 1.0 wt.% CeO_2 .

Table 2. EDS analysis results of Ni-based tungsten carbide cladding layer under different CeO_2 contents in Figure 4 (wt.%).

Spectrum	Ni	Cr	B	Si	Fe	C	W	Ce	Possible Phase
1	0.72	—	—	—	—	16.67	82.61	—	Tungsten carbide
2	16.57	6.88	—	0.21	0.65	13.71	61.98	—	SiC, WC, W_2C
3	38.06	9.22	—	—	1.36	9.75	41.59	—	M_{23}C_6
4	21.44	12.19	0.75	3.33	1.07	7.86	53.35	—	Tungsten carbide, SiC, WC, W_2C
5	74.83	3.29	1.91	0.28	4.44	13.32	1.93	—	γ -Ni solid solution
6	9.79	59.53	—	—	3.43	16.40	7.69	1.00	M_{23}C_6

As can be seen from the results in Table 2, in the spectrum 1 area, the content of the C element was 16.67 wt.%, the content of W was 82.61 wt.%, and there was a small amount of Ni, indicating tungsten carbide particles. In the edge zone spectrum 2, it contained the C of 13.71 wt.%, W of 61.98 wt.%, Ni of 16.57 wt.%, Cr of 6.88 wt.%, and a little of Si and Fe, which showed the secondary precipitated carbides. The spectrum 3 area around a tungsten carbide particle contained 9.75 wt.% C and a small amount of Fe, while was rich in W, Ni and Cr. It indicated M_{23}C_6 carbides formed. After adding CeO_2 into the powder, the spectrum 4 area represented tungsten carbide particles or the secondary precipitated carbides (SiC and WC, W_2C carbides). In the spectrum 5 area, it contained 74.83 wt.% Ni element, and a small amount of Cr, B, Si, Fe, W, and Ce. This region represented a Ni-based solid solution. In the spectrum 6 area, Ce element was detected.

Therefore, the addition of CeO_2 into the powder plays a critical role in the dissolution of tungsten carbide particles and the formation of secondary carbides in the cladding layer. On the one hand, an appropriate amount of CeO_2 can promote the dissolution of tungsten carbide and spheroidize tungsten carbide particles. Under the action of high-temperature plasma arc, CeO_2 in the powder is decomposed into Ce and O atom, meanwhile the tungsten carbide particles also begin to dissolve partially. Ce as a surface-active element, is easily adsorbed on the surface of tungsten carbide. However, owing to the large atomic radius of Ce, it is difficult to act with Fe, Ni, Cr, and other elements to form a solid solution (while it is easy to segregate at the grain boundary of tungsten carbide, which promotes the dissolution and spheroidization of tungsten carbide). On the other hand, Ce compounds can be used as heterogeneous nuclei to induce the formation of carbides, which spheroidize

and refine carbides. According to the previous thermodynamic calculation on the system of Ce-O-S [8], Ce_2O_3 precipitates preferentially. It is used as the heterogeneous nucleation core to induce the formation of M_{23}C_6 ($\text{M} = \text{Cr}, \text{Fe}, \text{Ni}, \text{W}$) carbides, secondary precipitates phases (SiC and $\text{WC}, \text{W}_2\text{C}$). Meanwhile, the active Ce is adsorbed at the grain boundaries of these carbides, which reduces the Gibbs free energy of the whole system and the driving force of carbides growth [16], thereby inhibiting the growth of carbides. With the increase of Ce content in the powder, the dissolved amount of tungsten carbide and the number of M_{23}C_6 carbides and secondary precipitate carbides increased. When the CeO_2 content was 0.2 wt.%, the tungsten carbide particles and carbides became spherical and were uniformly and finely dispersed in the cladding layer. When the CeO_2 content was increased further, excessive CeO_2 , which has a high melting point, increased the viscosity of the solution to reduce the dissolution rate of tungsten carbide particles. Gradually, the spheroidization and refinement effect of CeO_2 on the microstructure in the cladding layer was weakened, and the carbides formed in microstructure shows bar-like or rod-like shapes. The action mechanism model of CeO_2 in the Ni-based tungsten carbide cladding layer is shown in Figure 5.

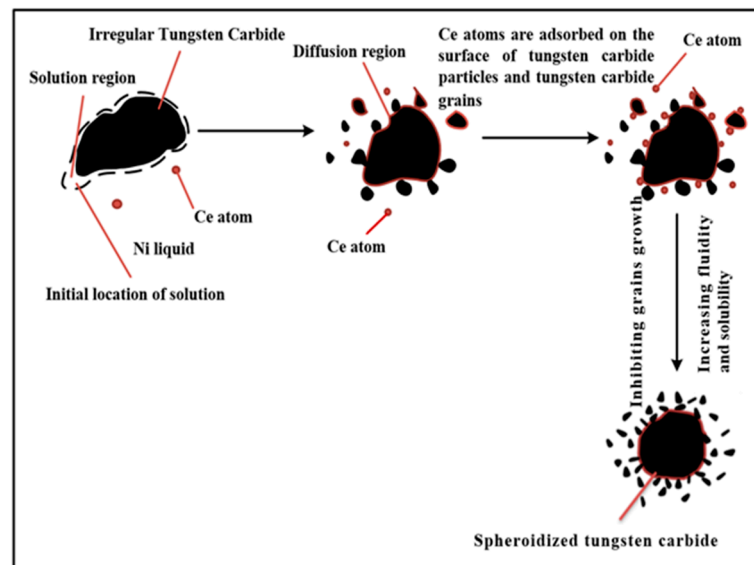


Figure 5. The mechanism model of the CeO_2 in Ni-based tungsten carbide cladding layer.

3.2. Effect of CeO_2 Content on Hardness of Ni-Based Tungsten Carbide Cladding Layer

Figure 6 shows the hardness of Ni-based tungsten carbide cladding layers under different CeO_2 contents. The average hardness of the cladding layer was 965 HV_{10} without CeO_2 in the powders. After adding CeO_2 into the powder, the hardness of the cladding layer increased first and then decreased with the increase of CeO_2 content. When the CeO_2 content was 0.2 wt.%, the average hardness value of the cladding layer reached the maximum of 1062 HV_{10} , which was 10% higher than that of the cladding layer without CeO_2 content. When the CeO_2 content was more than 0.2 wt.%, the hardness of the cladding layer decreased slightly. The average hardness value of the cladding layer was 915 HV_{10} with the CeO_2 content of 1.0 wt.%.

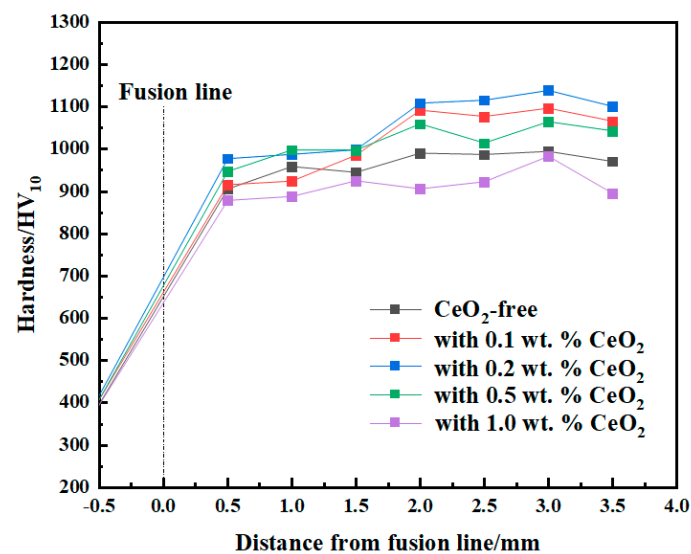


Figure 6. Hardness of the Ni-based tungsten carbide cladding layer with different CeO₂ contents.

Under the action of the plasma arc, firstly, the undissolved tungsten carbide plays a dispersion strengthening role in the cladding layer. Secondly, elements such as Cr, Si, Fe, and W are dissolved in the matrix to form Ni-based solid solution, which plays a solid solution strengthening role in the cladding layer. Thirdly, elements Ni, Cr, Si, Fe, W, B, and C form carbides and boride, and these hard phases play a precipitation strengthening role in the cladding layer [17]. The above strengthening effects lead to the high hardness of Ni-based tungsten carbide cladding layer. After adding CeO₂ into the powder, the number of Ce-containing compounds as nucleation particles increases with the increase of CeO₂ content, promoting the dispersion of carbides in the cladding layer. Moreover, the carbides in the cladding layer are spheroidized. When the CeO₂ content was 0.2 wt.%, the refinement and spheroidization effect of CeO₂ reached the optimum, resulting in the highest hardness of the cladding layer. However, if the CeO₂ content was 0.5 wt.% and 1.0 wt.%, Ce-containing compounds as nucleation particles grew and most of them were removed as a molten slag, and the viscosity of the solution was increased, so the refinement and spheroidization effect of CeO₂ was weakened, leading to the decrease of the hardness of the cladding layer.

It also indicated that whether the powder contained CeO₂ or not, the hardness maximum of the cladding layer was located at a distance of 3.0 mm away from the substrate. Works in the literature [18] have studied the effect of different tungsten carbide contents on the hardness of Ni-based tungsten carbide cladding layer obtained by plasma arc cladding technology. The results showed that when the tungsten carbide content in the powder was 35%, the number of tungsten carbide particles in the cladding layer increased significantly and became distributed mainly at a distance of 2.5–3.5 mm from the substrate, resulting in the highest hardness of cladding layer. Our conclusions confirmed the above research result.

3.3. Effect of CeO₂ on Wear Resistance of Ni-Based Carbide Cladding Layer

The friction coefficient and the wear rate of the cladding layer are two important indicators for evaluating the wear resistance of the cladding layer. Figure 7a,b show the variation curve of friction coefficient with time and wear rate of cladding layer under different CeO₂ contents, respectively. When the powder did not contain CeO₂, the average friction coefficient of the cladding layer was 0.622 and its wear rate was 0.0062 mg/m. When adding 0.2 wt.% CeO₂ into the powder, the average friction coefficient of the cladding layer decreased significantly and reached the minimum of 0.502, similarly, the corresponding wear rate was 0.0018 mg/m, which decreased by 71% compared with the sample without CeO₂. When the CeO₂ content was increased to 1.0 wt.%, the average friction coefficient of

the cladding layer was raised to 0.582, while its wear rate was increased to 0.0060 mg/m. The change trend of wear resistance is consistent with hardness for the cladding layer. Based on Holm-Archard wear theory [19], the hardness of the material has a linear relationship with wear loss. The higher the hardness of the material, the smaller the wear rate. The theory confirms the above result. Meanwhile, it indicated that adding 0.2 wt.% CeO₂ into the powder, can refine the microstructure of the cladding layer, so that the corresponding wear resistance reaches an optimum value.

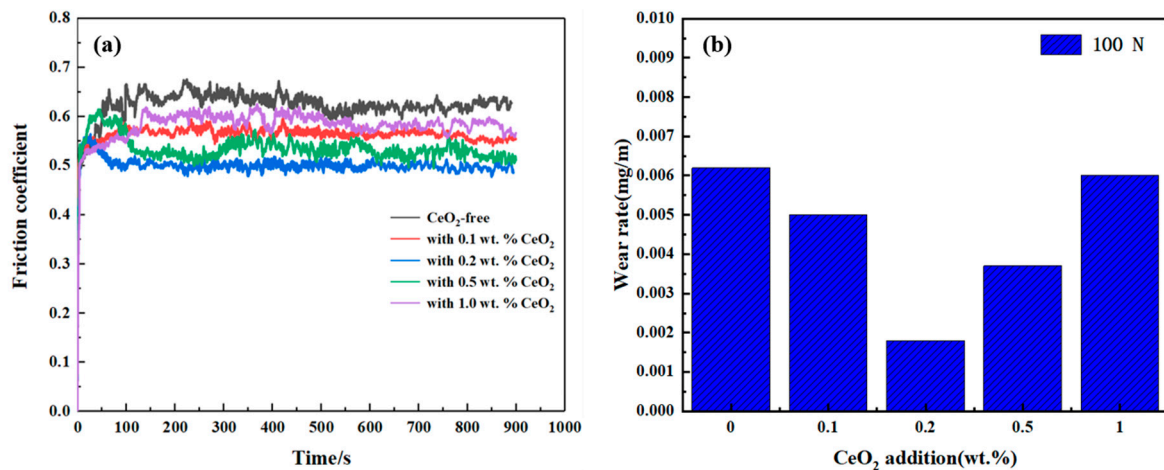


Figure 7. The wear resistance of the cladding layer under different CeO₂ content: (a) variation curve of friction coefficient with time, (b) wear rate.

Figure 8 shows morphologies of Ni-based tungsten carbide cladding layer with different CeO₂ contents after wear. If the powder did not contain CeO₂, the cladding layer presented noticeable furrow-like wear marks, and its surface contained some adhesions. When the CeO₂ content in the powder did not exceed 0.2 wt.% (see Figure 8b,c), the furrow-like wear marks on the surface of the cladding layer basically disappeared while tungsten carbide particles and carbides were exposed at the location of wear marks. When the CeO₂ content in the powder was increased to 0.5 wt.% and 1.0 wt.%, furrow-like wear marks and adhesives appeared again in the cladding layer (see Figure 8d,e).

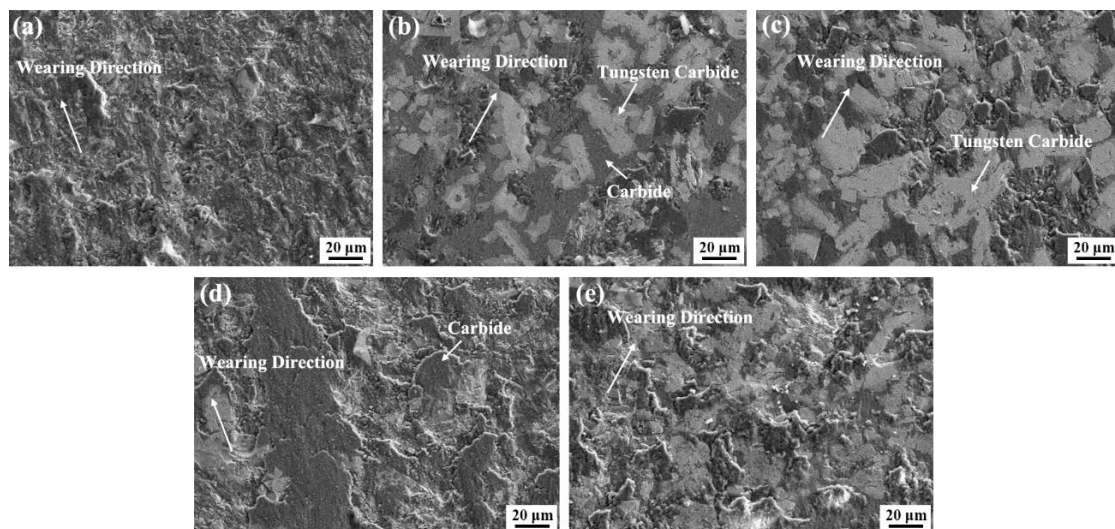


Figure 8. Morphologies of Ni-based tungsten carbide cladding layer after wear under different CeO₂ contents: (a) 0 wt.% CeO₂, (b) 0.1 wt.% CeO₂, (c) 0.2 wt.% CeO₂, (d) 0.5 wt.% CeO₂, and (e) 1.0 wt.% CeO₂.

During the friction and wear test, the hardness and wear resistance of the Ni-based solid solution are much lower than those of the tungsten carbide particles and carbides in the cladding layer. Therefore, Ni-based alloy preferentially produces wear loss and concave under the friction of hard abrasive materials, then the tungsten carbide particles and carbide particles expose gradually. Finally, these carbide particles act as a skeleton during wear, which reduces the loss of Ni-based alloy. Actually, an Ni-based alloy can support tungsten carbides and carbides due to its high toughness and prevent tungsten carbides and carbides from falling off. The cladding layer presents good wear resistance. When adding the appropriate amount of CeO₂ into the powder, the number of carbide particles increased, and it distributed dispersively. The cladding layer had the best wear resistance. Some works in the available literature also agree with this view [20,21].

4. Conclusions

In this study, Ni-based tungsten carbide surfacing layer was prepared on the surface of Q345 steel by plasma arc cladding technology. The effect of CeO₂ content on the microstructure and properties of the cladding layer was studied. The main conclusions are as follows:

(1) Whether CeO₂ was added into the powder or not, the microstructure was mainly composed of γ -Ni solid solution, tungsten carbide particles and carbides. After adding CeO₂ into the powder, the tungsten carbide which was partially dissolved, shaped from irregular into spherical and became fine, while the number of secondary precipitation carbides increased and it distributed uniform in the cladding layer. When the CeO₂ content was 0.2 wt.%, the spheroidization and refinement effect were optimum. As the CeO₂ content exceeded 0.2 wt.%, the shape of the tungsten carbide reverted to an irregular shape and the secondary precipitation carbide became bar-like or rod-like shapes.

(2) After adding an appropriate amount of CeO₂ into the powder, on the one hand, the Ce atoms were adsorbed on the surface of the tungsten carbide, which was dissolved and spheroidized. On the other hand, the preferentially formed Ce-containing alloy induced the formation of secondary precipitation carbides, resulting in the refinement of the microstructure. However, as the CeO₂ addition was excessive, the viscosity of the solution increased, leading to the composition segregation. Thus, the spheroidization and refinement of CeO₂ on the cladding layer were weakened.

(3) With the increase of CeO₂ content, the hardness and wear resistance of the cladding layer increased first and then decreased. When the CeO₂ content was 0.2 wt.%, the average hardness value of the cladding layer reached the maximum of 1062 HV₁₀, and the corresponding wear resistance of the cladding layer reach an optimum value.

Author Contributions: Conceptualization: J.P., W.-M.L. and P.H.; methodology: Y.-B.S. and J.P.; formal analysis: J.P. and L.W.; resources: W.-M.L.; data curation: L.W.; writing—original draft preparation: J.P. and Y.-B.S.; writing—review and editing: J.P. and W.-M.L.; writing—manuscript finalization: J.P., W.-M.L. and P.H.; supervision: J.P. and W.-M.L.; project administration: W.-M.L.; funding acquisition: W.-M.L. All authors have read and agreed to the published version of the manuscript.

Funding: This research was supported by State Key Laboratory of Advanced Brazing Filler Metals and Technology, the Natural Science Foundation of Jiangsu Province (Grant No. BK20191458), the Technology and Innovation Program for Undergraduates of Jiangsu University of Science and Technology, the Research and Practice innovation plan for Postgraduates in Jiangsu Province (No. SJCX 20-1457), and the open research foundation of the State Key Laboratory of Advanced Welding and Joining (No. AWJ-21M15).

Institutional Review Board Statement: Not applicable.

Informed Consent Statement: Not applicable.

Data Availability Statement: Not applicable.

Conflicts of Interest: The authors declare no conflict of interest. The funder had no role in the design of the study; in the collection, analyses, or interpretation of data; in the writing of the manuscript; or in the decision to publish the results.

References

1. Xun, S.B.; Wang, B.; Zhang, L.; Long, W.M. Development of Green Welding Technology in China During the Past Decade. *Mater. Rep.* **2019**, *33*, 2813–2830.
2. Xu, B.S.; Ma, S.N.; Liu, S.C.; Zhang, W. Remanufacturing engineering in 21st century. *China Mech. Eng.* **2000**, *101*, 45–48.
3. Yang, Q.T. *The Design of Differential Shells' Remanufacturing Production Line Based on Surfacing*; Guangxi University: Nanning, China, 2015.
4. Xie, G.Z.; Song, X.L.; Zhang, D.J.; Wu, Y.P.; Liu, P.H. Microstructure and corrosion properties of thick WC composite coating formed by plasma cladding. *Appl. Surf. Sci.* **2010**, *256*, 6354–6358.
5. Xu, G.J.; Muneharu, K.; Liu, Z.J.; Zhang, H. Characteristics of Ni-based coating layer formed by laser and plasma cladding processes. *Mater. Sci. Eng. A* **2005**, *417*, 63–72. [[CrossRef](#)]
6. He, Y.Z.; Si, S.H.; Xu, K.; Yuan, X.M. Effect of Cr₃C₂ particles on microstructure and corrosion-wear resistance of laser cladding Co-based alloy coating. *Chinese J. Lasers* **2004**, *31*, 1143–1148.
7. Zhou, F.; Hou, Q.Y. Microstructure and wear resistance of plasma arc cladding Y₂O₃/Cobalt-based alloy coating. *Rare Metal. Mat. Eng.* **2008**, *37*, 294–298.
8. Pu, J.; Yu, S.F.; Li, Y.Y. Role of inclusions in flux aided backing submerged arc welding. *J. Mater. Process. Technol.* **2017**, *240*, 145–153. [[CrossRef](#)]
9. Pu, J.; Xue, S.B.; Zhang, L.; Wu, M.F.; Long, W.M.; Wang, S.Q.; Qian, S.J.; Lin, T.S. Effect of CeO₂ on Wettability of Ag₃₀CuZnSn Flux Cored Brazing Filler Metal and Microstructure and Properties of Brazed Joint. *Mater. Rep.* **2021**, *35*, 08134–08139.
10. Shi, Y.; Du, X.D.; Zhuang, P.C.; Wang, C.J.; Gao, W.D. Research and development trend of plasma cladding technology. *Surf. Technol.* **2019**, *48*, 23–33.
11. Wang, C.L.; Zhang, G.Y.; Gao, Y.; Song, Y.Z. Mechanism of Y₂O₃ affecting laser cladding of Ni-based coating on 6063 Al alloy substrate. *Chin. J. Rare Met.* **2016**, *40*, 201–206.
12. He, K.S.; Cheng, X.Y.; Li, Z.H. Surface modification on cermet coating microstructure by rare earths and its application development. *Lubr. Eng.* **2009**, *34*, 100–104.
13. Li, D.K.; Li, M.X.; Hong, H.F.; Gao, H.H.; Wang, G.L. Effect of CeO₂ on microstructure and properties of Fe-based coating produced by plasma arc cladding process. *Trans. China Weld. Inst.* **2011**, *32*, 109–112, 118.
14. Zhang, G.Y.; Wang, C.L.; Gao, Y.; Song, Y.Z. Effect of rare earth on the microstructure and tribological properties of laser cladding Ni-based coatings on 6063 Al. *Tribology* **2015**, *35*, 335–341.
15. Zhou, Y.F.; Yang, Y.L.; Jiang, Y.W.; Yang, J.; Ren, X.J.; Yang, Q.X. Fe-24 wt.%Cr-4.1 wt.%C hardfacing alloy: Microstructure and carbide refinement mechanisms with ceria additive. *Mater. Charact.* **2012**, *72*, 77–86. [[CrossRef](#)]
16. Wang, C.L.; Gao, Y.; Zeng, Z.C.; Fu, Y.K. Effect of rare-earth on friction and wear properties of laser cladding Ni-based coatings on 6063Al. *J. Alloys Compd.* **2017**, *727*, 278–285. [[CrossRef](#)]
17. Li, S.T.; Liu, S.S.; Chen, H.Y.; Dong, L.H.; Yin, Y.S. Wear resistance of PTAW deposited Ni-based WC composite coating. *Surf. Technol.* **2018**, *47*, 103–110.
18. Wu, L.; Pu, J.; Wu, M.F.; Long, W.M.; Zhong, S.J.; Hu, Q.X.; Lan, Y. Effects of different tungsten carbide contents on microstructure and properties of Ni-based tungsten carbide cladding layer by plasma arc cladding technology. *Mater. Rep.* **2021**, *35*, 16111–16114.
19. Li, M.Y.; Han, B.; Wang, Y.; Song, L.X. Effect of ultrasonic vibration on microstructure and property of laser cladding Ni55 coating. *Trans. Mater. Heat Treat.* **2015**, *36*, 199–203.
20. Chen, J.; Xiao, X.J. Effect of CeO₂ on microstructure and performance of WC-Co Ni-based composite coatings produced by laser cladding. *Surf. Technol.* **2011**, *40*, 29–31.
21. Liu, X.B.; Wang, H.M. Effects of La₂O₃ on microstructure and properties of laser clad γ /Cr₇C₃/TiC composite coatings on TiAl intermetallic alloy. *Chin. J. Lasers* **2005**, *262*, 1011–1016.